PHYSICAL REVIEW D **93,** 014016 (2016)

Watson's theorem and the $N\Delta(1232)$ axial transition

L. Alvarez-Ruso,[1] E. Hernández,[2] J. Nieves,[1] and M. J. Vicente Vacas[3]
[1]*Instituto de Física Corpuscular (IFIC), Centro Mixto CSIC-Universidad de Valencia, Institutos de Investigación de Paterna, E-46071 Valencia, Spain*
[2]*Departamento de Física Fundamental e IUFFyM, Universidad de Salamanca, E-37008 Salamanca, Spain*
[3]*Departamento de Física Teórica and IFIC, Centro Mixto Universidad de Valencia-CSIC, Institutos de Investigación de Paterna, E-46071 Valencia, Spain*
(Received 21 October 2015; published 15 January 2016)

We present a new determination of the $N\Delta$ axial form factors from neutrino induced pion production data. For this purpose, the model of Hernandez *et al.* [Phys. Rev. D 76, 033005 (2007)] is improved by partially restoring unitarity. This is accomplished by imposing Watson's theorem on the dominant vector and axial multipoles. As a consequence, a larger $C_5^A(0)$, in good agreement with the prediction from the off-diagonal Goldberger-Treiman relation, is now obtained.

DOI: 10.1103/PhysRevD.93.014016

I. INTRODUCTION

Weak pion production off nucleons provides valuable insight into the axial structure of hadrons. In addition, pion production cross sections grow to become one of the main reaction mechanisms for neutrinos of few-GeV energies, which is an important range for current and future oscillation experiments. Therefore, a better understanding of weak pion production mechanisms is actively pursued [1–3]. Recent measurements on, predominantly, carbon targets by MiniBooNE [4–6] and MINERvA [6,7] experiments have revealed discrepancies with existing theoretical models and among different data sets [8–12].

The first requirement to achieve a precise knowledge of neutrino induced pion production on nuclear targets is a realistic model at the nucleon level. Theoretical studies of weak pion production off the nucleon at intermediate energies [13–42] have highlighted the important role of baryon resonance excitation, predominantly the $\Delta(1232)3/2^+$. The weak nucleon-to-$\Delta(1232)$ transition current can be written in terms of vector and axial form factors, C_{3-5}^V and C_{3-6}^A in the notation of Ref. [16]. Although there are quark model determinations of these form factors [26,43–45], a common strategy is to adopt empirical parametrizations for them. The role of heavier resonances has also been investigated, although the available experimental information about the axial sector is very limited. Among these states, only the $N(1520)3/2^-$ appears to be relevant for neutrino energies below 1.5 GeV [33]. Nonresonant electroweak amplitudes have also been extensively considered. As pointed out in Ref. [31], these terms are not only demanded but, close to threshold, fully fixed by chiral symmetry. Away from threshold, these amplitudes are usually modeled using phenomenologically parametrized nucleon form factors, introduced in a way that respects both the conservation of the vector current (CVC) and the partial conservation of the axial current (PCAC).

In Ref. [31] (referred from now on as the HNV model), nonresonant amplitudes, evaluated from the leading contributions of the SU(2) chiral Lagrangian, supplemented with empirical parametrizations of the nucleon form factors, were considered alongside the $\Delta(1232)$ excitation. The vector form factors in the $N\Delta$ vertex come from helicity amplitudes extracted in the analysis of electron scattering data [29]. The most important among the axial form factors is C_5^A, which appears at leading order in an expansion of the hadronic tensor in the 4-momentum transfer q^2. Assuming the pion pole dominance of the pseudoscalar form factor C_6^A, it can be related to C_5^A owing to PCAC. For the subleading $C_{3,4}^A$ form factors, Adler's parametrizations [13,14] were adopted: $C_3^A = 0$, $C_4^A = -C_5^A/4$. The available bubble-chamber data on pion production induced by neutrinos on deuterium, taken at Argonne and Brookhaven National Laboratories (ANL and BNL) [46,47] are quite insensitive to the values of these form factors [36]. With the aim of extending the model toward higher energies, the $N(1520)$ intermediate state was added in Ref. [9] using the transition form factors introduced in Ref. [33].

The pion pole dominance of C_6^A and PCAC result in a relation between the leading axial coupling $C_5^A(q^2 = 0)$ and the $\Delta \to N\pi$ decay coupling known as the off-diagonal Goldberger-Treiman relation (GTR). Studies that neglected the nonresonant contributions found good agreement between the $C_5^A(0)$ value extracted from ANL and/or BNL data and the GTR [24,35]. However, the fit of $C_5^A(q^2)$ to the flux averaged $\nu_\mu p \to \mu^- p\pi^+$ ANL q^2-differential cross section data [46] with the HNV model found a discrepancy of 30% with respect to the GTR prediction of $C_5^A(0) = 1.15 - 1.2$. A simultaneous fit to both ANL and BNL data samples including independent overall flux normalization uncertainties for each experiment, as suggested in Ref. [35], and considering deuterium-target corrections

obtained $C_5^A(0) = 1.00 \pm 0.11$ [36], still 2σ below the GTR value. Although the HVN model could be reconciled with the GTR by simultaneously fitting vector form factors to electron-proton scattering structure function F_2 [40,48], it should be realized that the HNV model does not satisfy Watson's theorem [49]. The latter, which is a consequence of unitarity and time-reversal invariance, implies that the phase of the electroweak pion production is fully determined by the strong πN interaction. The goal of the present study is to impose Watson's theorem in the HNV model. It is shown that, in this way, the consistency with the GTR prediction is restored.

The dynamical model of photo-, electro-, and weak pion production derived in Ref. [27] deserves a special mention. To date, this is the only weak pion production model fulfilling Watson's theorem exactly. Starting from an effective Hamiltonian with bare $N\Delta$ couplings obtained in a nonrelativistic constituent quark model [22], the Lippmann-Schwinger equation in coupled channels is solved, which restores unitarity. Besides, the bare couplings get renormalized by meson clouds. The predicted cross sections are in good agreement with data (Figs. 5–8 of Ref. [27]). The scheme has been further refined and extended to incorporate N^* resonances and a larger number of meson-baryon states [41,50]. Although the chiral counting at threshold is broken by the presence of ρ and ω exchanges in the t channel or the introduction of explicit σ meson intermediate states, this framework should satisfy unitary constraints and fulfill Watson's theorem. The partially unitarized HNV model presented here is considerably simpler. The agreement with the GTR and a good description of data for invariant masses $W_{\pi N} < 1.4$ GeV are achieved by introducing two relative phases between the $\Delta(1232)$ and the nonresonant contributions. The HNV model improved in this way is portable and can be easily implemented in event generators used in the analysis of neutrino oscillation experiments.

The paper is organized as follows. In Sec. II, we introduce Watson's theorem, which is based on unitarity and time reversal invariance, and explain its implementation in the HNV model. In Sec. III, we present the new extraction of the $C_5^A(q^2)$ axial form factor. Appendices A, B, and C collect some useful formulas needed for the calculation. Finally, in Appendix D, we give a parametrization of the Olsson phases (see below) used to impose Watson's theorem in our approach.

II. UNITARITY, TIME-REVERSAL INVARIANCE, AND WATSON'S THEOREM

A scattering process due to short-range interactions (like strong or weak interactions) can be described in terms of initial and final states of noninteracting particles. The amplitude for a transition is given by the corresponding matrix element of the scattering operator

$$S = \mathbb{1} - iT. \tag{1}$$

Given an initial state $|I\rangle$, the probability for finding the system in an asymptotic state $|N\rangle$ is $P_N = |\langle N|S|I\rangle|^2$; since $\sum_N P_N = 1$, one deduces that S is a unitary operator, $SS^\dagger = S^\dagger S = \mathbb{1}$, which implies that[1]

$$\begin{aligned} i(T - T^\dagger) &= T^\dagger T \\ i\{\langle F|T|I\rangle - \langle F|T^\dagger|I\rangle\} &= \langle F|T^\dagger T|I\rangle \\ &= \sum_N \langle F|T^\dagger|N\rangle\langle N|T|I\rangle \\ &= \sum_N \langle N|T|F\rangle^*\langle N|T|I\rangle. \end{aligned} \tag{3}$$

On the other hand, if time reversal invariance holds,

$$\langle F|S|I\rangle = \langle I_{\mathcal{T}}|S|F_{\mathcal{T}}\rangle, \tag{4}$$

where $\mathcal{T}|I\rangle = |I_{\mathcal{T}}\rangle$ and $\mathcal{T}|F\rangle = |F_{\mathcal{T}}\rangle$. In other words, if the system is time reversal invariant, $\mathcal{T}S\mathcal{T}^\dagger = S^\dagger$ and therefore $\mathcal{T}^\dagger T^\dagger \mathcal{T} = T$. The time reversal operator $\mathcal{T}$ is antiunitary[2] [51,52] with $\mathcal{T}^2 = \pm\mathbb{1}$. Thus, one finds

$$\begin{aligned} \langle F|T^\dagger|I\rangle &= \langle I|T|F\rangle^* \\ &= \langle I|\mathcal{T}^\dagger T^\dagger \mathcal{T}|F\rangle^* \\ &= \langle I_{\mathcal{T}}|T^\dagger|F_{\mathcal{T}}\rangle \\ &= \langle F_{\mathcal{T}}|T|I_{\mathcal{T}}\rangle^*. \end{aligned} \tag{5}$$

Using this result in Eq. (3), we obtain from unitarity and time reversal invariance that

$$i\{\langle F|T|I\rangle - \langle F_{\mathcal{T}}|T|I_{\mathcal{T}}\rangle^*\} = \sum_N \langle N|T|F\rangle^*\langle N|T|I\rangle. \tag{6}$$

If $\langle F|T|I\rangle = \langle F_{\mathcal{T}}|T|I_{\mathcal{T}}\rangle$, which is always satisfied for transitions between c.m. two-particle states with well-defined helicities and total angular momentum whenever the interaction is invariant under time reversal [51], and there is only one relevant intermediate state in the sum of Eq. (6), one obtains that

$$\langle N|T|F\rangle^*\langle N|T|I\rangle = -2\mathrm{Im}\langle F|T|I\rangle \in \mathbb{R} \tag{7}$$

so that the phases of $\langle N|T|F\rangle$ and $\langle N|T|I\rangle$ coincide. This result constitutes Watson's theorem [49] on the effect of final state interactions on reaction cross sections. As shown, it is a consequence of unitarity and time reversal invariance.

[1]The optical theorem trivially follows from the particular case $|I\rangle = |F\rangle$,

$$\mathrm{Im}\langle I|T|I\rangle = -\frac{1}{2}\sum_N |\langle N|T|I\rangle|^2. \tag{2}$$

[2]This is to say antilinear, $\langle A_{\mathcal{T}}|O|B_{\mathcal{T}}\rangle = \langle A|\mathcal{T}^\dagger O\mathcal{T}|B\rangle^*$, and satisfying $\mathcal{T}^{-1} = \mathcal{T}^\dagger$.

A. Watson's theorem for c.m. two-particle helicity states

Assuming that only two-particle intermediate states (2body), with masses m_1' and m_2', contribute[3], the unitarity condition of Eq. (3) for the binary process $a+b\to 1+2$ can be written as

$$i\{\langle\theta,\varphi;\lambda_1,\lambda_2;\gamma_{12}|T(s)|0,0;\lambda_a,\lambda_b;\gamma_{ab}\rangle-\langle\theta,\varphi;\lambda_1,\lambda_2;\gamma_{12}|T^\dagger(s)|0,0;\lambda_a,\lambda_b;\gamma_{ab}\rangle\}$$
$$=\sum_{2\text{body}}\frac{\lambda^{1/2}(s,m_1'^2,m_2'^2)}{32\pi^2 s}\int d\Omega'\sum_{\gamma_{12}'}\sum_{\lambda_1'\lambda_2'}\langle\theta',\varphi';\lambda_1',\lambda_2';\gamma_{12}'|T(s)|\theta,\varphi;\lambda_1,\lambda_2;\gamma_{12}\rangle^*\langle\theta',\varphi';\lambda_1',\lambda_2';\gamma_{12}'|T(s)|0,0;\lambda_a,\lambda_b;\gamma_{ab}\rangle, \tag{8}$$

where $s=(p_a+p_b)^2$ and the function $\lambda(x,y,z)=x^2+y^2+z^2-2xy-2xz-2yz$. Two-particle states in the c.m. are defined in Appendix A. The matrix element of the T operator is computed in the little Hilbert space (see Appendix A and Ref. [51]),

$$\langle\theta,\varphi;\lambda_1,\lambda_2;\gamma_{12}|T(s)|0,0;\lambda_a,\lambda_b;\gamma_{ab}\rangle\equiv\langle\alpha_F|T_P|\alpha_I\rangle=\frac{(2\pi)^2 4\sqrt{s}}{\sqrt{|\vec{p}_I||\vec{p}_F|}}\langle\theta,\varphi;\lambda_1,\lambda_2;\gamma_{12}|T_P|0,0;\lambda_a,\lambda_b;\gamma_{ab}\rangle\equiv T_{FI}(s), \tag{9}$$

where $|\vec{p}_{I(F)}|\equiv|\vec{p}_{a(1)}|=|\vec{p}_{b(2)}|$; T_P is the reduction of the full operator T in the little Hilbert space, Eq. (A12). Normalizations are fixed by the expression of the c.m. differential cross section for the $a+b\to 1+2$ reaction, which is calculated as

$$\frac{d\sigma}{d\Omega}=\frac{1}{64\pi^2 s}\frac{|\vec{p}_F|}{|\vec{p}_I|}|T_{FI}(s)|^2. \tag{10}$$

The unitarity condition, Eq. (8), can be rewritten for states $|J,M\rangle$ with well-defined angular momentum. Changing basis with Eq. (A16) and using the orthogonality properties of the $\mathcal{D}^{(J)}_{MM'}(\varphi,\theta,-\varphi)$ rotation matrices [Eq. (A18)], the condition $\mathcal{D}^{(J)}_{MM'}(0,0,0)=\delta_{MM'}$, the fact that T is a scalar under rotations, and Parseval's identity associated to Eq. (A14), one gets that

$$i\{\langle J,M;\lambda_1,\lambda_2;\gamma_{12}|T(s)|J,M;\lambda_a,\lambda_b;\gamma_{ab}\rangle-\langle J,M;\lambda_1,\lambda_2;\gamma_{12}|T^\dagger(s)|J,M;\lambda_a,\lambda_b;\gamma_{ab}\rangle\}$$
$$=\sum_{2\text{body}}\frac{\lambda^{1/2}(s,m_1'^2,m_2'^2)}{32\pi^2 s}\sum_{\gamma_{12}'}\sum_{\lambda_1'\lambda_2'}\langle J,M;\lambda_1',\lambda_2';\gamma_{12}'|T(s)|J,M;\lambda_1,\lambda_2;\gamma_{12}\rangle^*\langle J,M;\lambda_1',\lambda_2';\gamma_{12}'|T(s)|J,M;\lambda_a,\lambda_b;\gamma_{ab}\rangle, \tag{11}$$

with $M=\lambda_a-\lambda_b$ as follows from Eq. (A15). In practice, all the above matrix elements do not depend on M because T is a scalar under rotations. Hence, it is usual to adopt the short notation

$$\langle J,M;\lambda_1,\lambda_2;\gamma_{12}|T(s)|J,M;\lambda_a,\lambda_b;\gamma_{ab}\rangle=\langle\lambda_1,\lambda_2;\gamma_{12}|T_J(s)|\lambda_a,\lambda_b;\gamma_{ab}\rangle. \tag{12}$$

Assuming time reversal invariance ($\mathcal{T}^\dagger T\mathcal{T}=T^\dagger$),

$$\langle\lambda_1,\lambda_2;\gamma_{12}|T_J^\dagger(s)|\lambda_a,\lambda_b;\gamma_{ab}\rangle=\langle\lambda_1,\lambda_2;\gamma_{12}|\mathcal{T}^\dagger T_J(s)\mathcal{T}|\lambda_a,\lambda_b;\gamma_{ab}\rangle=\langle\lambda_1,\lambda_2;\gamma_{12}|T_J(s)|\lambda_a,\lambda_b;\gamma_{ab}\rangle^*, \tag{13}$$

since $\mathcal{T}$ is an antiunitary operator. We have also used the transformation properties under time reversal of the helicity $|J,M;\lambda,\lambda';\gamma\rangle$ states[4]:

$$\mathcal{T}|J,M;\lambda_1,\lambda_2;\gamma\rangle=(-1)^{J-M}|J,-M;\lambda_1,\lambda_2;\gamma\rangle. \tag{14}$$

[3]This is exact below the three-particle threshold.

[4]To obtain Eq. (14), the intrinsic time reversal parities of all involved particles have been set to $+1$ (see Ref. [51]). Within the conventions used in Ref. [31] (HNV model), this is not the case for the pion, which should be taken into account in the following (see the discussion in Appendix C).

Thus, the left-hand side of Eq. (11) becomes

$$i\{\langle\lambda_1,\lambda_2;\gamma_{12}|T_J(s)|\lambda_a,\lambda_b;\gamma_{ab}\rangle-\langle\lambda_1,\lambda_2;\gamma_{12}|T_J^\dagger(s)|\lambda_a,\lambda_b;\gamma_{ab}\rangle\}=-2\mathrm{Im}\langle\lambda_1,\lambda_2;\gamma_{12}|T_J(s)|\lambda_a,\lambda_b;\gamma_{ab}\rangle. \tag{15}$$

Hence, (provided time reversal invariance holds) one finds

$$\begin{aligned}\mathrm{Im}\langle\lambda_1,\lambda_2;\gamma_{12}|T_J(s)|\lambda_a,\lambda_b;\gamma_{ab}\rangle=&-\frac{1}{2}\sum_{2\mathrm{body}}\frac{\lambda^{1/2}(s,m_1'^2,m_2'^2)}{32\pi^2 s}\\&\times\sum_{\gamma_{12}'}\sum_{\lambda_1'\lambda_2'}\langle\lambda_1',\lambda_2';\gamma_{12}'|T_J(s)|\lambda_1,\lambda_2;\gamma_{12}\rangle^*\langle\lambda_1',\lambda_2';\gamma_{12}'|T_J(s)|\lambda_a,\lambda_b;\gamma_{ab}\rangle.\end{aligned} \tag{16}$$

Let us consider an electroweak transition from an initial state $(a+b)$ involving at least a gauge boson to a purely hadronic final state $(1+2)$. Furthermore, let us assume that the total c.m. energy, $\sqrt{s}$, is such that the only relevant strong process is the elastic one $1+2\to1+2$. In these circumstances, the sum over intermediate states in Eq. (16) is dominated by the $1+2\to1+2$ strong T matrix. The contribution of any other intermediate state will be proportional to the product of two electroweak transition amplitudes, and hence highly suppressed. Therefore,

$$\sum_{\gamma_{12}'}\sum_{\lambda_1'\lambda_2'}\langle\lambda_1',\lambda_2';\gamma_{12}'|T_J(s)|\lambda_1,\lambda_2;\gamma_{12}\rangle^*\langle\lambda_1',\lambda_2';\gamma_{12}'|T_J(s)|\lambda_a,\lambda_b;\gamma_{ab}\rangle\in\mathbb{R}, \tag{17}$$

which establishes a series of relations between the phases of the electroweak $a+b\to1+2$ and the strong $1+2\to1+2$ amplitudes.

B. Watson's theorem for $WN\to\pi N$ and $ZN\to\pi N$ amplitudes

Pion production off nucleons induced by (anti)neutrinos proceeds through charged (CC) or neutral current (NC) interactions. These are determined by transition amplitudes of the kind $WN\to\pi N$ and $ZN\to\pi N$, respectively. In the following, we explicitly refer to the CC case, but the extension to NC processes is straightforward. The off-shellness of the W boson does not alter the following arguments and will be reconsidered later on.

For the $WN\to\pi N$ reaction, considering only πN intermediate states, Eq. (17) becomes[5]

$$\sum_\rho\langle J,M;\underbrace{0,\rho}_{\pi N}|T(s)|J,M;\underbrace{0,\lambda'}_{\pi N}\rangle^*\langle J,M;\underbrace{0,\rho}_{\pi N}|T(s)|J,M;\underbrace{r,\lambda}_{WN}\rangle\in\mathbb{R},\qquad M=r-\lambda, \tag{18}$$

where r is the helicity of the W gauge boson and λ,λ',ρ are the corresponding helicities of the initial, final and intermediate nucleons. The above expression is equivalent to[6]

$$\sum_\rho\langle J,M;\underbrace{0,\rho}_{\pi N}|T(s)|J,M;\underbrace{0,\lambda'}_{\pi N}\rangle^*\langle J,M;\underbrace{0,\rho}_{\pi N}|T(s)|0,0;\underbrace{r,\lambda}_{WN}\rangle\in\mathbb{R}, \tag{19}$$

where we identify the initial WN pair with the z direction ($\theta=0,\varphi=0$) helicity c.m. two-particle state. Introducing states with well-defined orbital angular momentum L and spin S [Eq. (A20)], and using parity conservation on the $\pi N\to\pi N$ matrix elements, one gets

$$\sum_L\sum_\rho\frac{2L+1}{2J+1}(L,1/2,J|0,-\lambda',-\lambda')(L,1/2,J|0,-\rho,-\rho)\underbrace{\langle J,M;L,1/2|T(s)|J,M;L,1/2\rangle^*}_{\pi N\to\pi N}\underbrace{\langle J,M;0,\rho|T(s)|0,0;r,\lambda\rangle}_{WN\to\pi N}\in\mathbb{R}$$
$$\forall J,\quad M=r-\lambda. \tag{20}$$

Here, $(L,S,J|M_L,M_S,M_J)$ are Clebsch-Gordan coefficients.

[5]As the states are fully defined, the sum over γ_{12}' can be dropped.

[6]We use that $|0,0;r,\lambda\rangle=\sum_J\sqrt{\frac{2J+1}{4\pi}}|J,M=r-\lambda;r,\lambda\rangle$ and that T is a scalar.

C. Olsson's implementation of Watson's theorem for the $WN \to \pi N$ amplitude in the Δ region

At intermediate energies, the weak pion production off nucleons is dominated by the weak excitation of the $\Delta(1232)$ resonance and its subsequent decay into $N\pi$. Thus, for $J = 3/2$, isospin $I = 3/2$ ($W^+p \to \pi^+p$), and c.m. energies in the Δ region, the $L = 1$ partial wave in Eq. (20) should be the most important. Actually, it largely dominates the $\pi^+p \to \pi^+p$ reaction at these energies for $J = 3/2$. Its contribution is much larger than the one of the d wave, which is also allowed. Therefore, for the different r, λ values, but with fixed $M = r - \lambda$, the quantities $\chi_{r,\lambda}(s)$, defined as (we introduce the factor $\sqrt{3\pi/8}$ for latter convenience)

$$\chi_{r,\lambda}(s) = \sqrt{\frac{3\pi}{8}}\sum_{\rho}(1, 1/2, 3/2|0, -\rho, -\rho)\langle 3/2, M; 0, \rho|T(s)|0, 0; r, \lambda\rangle, \qquad M = r - \lambda, \tag{21}$$

should have the phase, $\delta_{P_{33}}(s)$, of the $L_{2J+1,2I+1} = P_{33}$ πN partial wave. Expressing the $|JM\rangle$ πN intermediate state in terms of helicity c.m. two-particle states [Eq. (A19)], we finally find

$$\chi_{r,\lambda}(s)e^{-i\delta_{P_{33}}} = \sqrt{\frac{3}{8}}\left(\sum_{\rho}(1, 1/2, 3/2|0, -\rho, -\rho)\int d\Omega \mathcal{D}^{(3/2)}_{M-\rho}(\varphi, \theta, -\varphi)\underbrace{\langle\theta, \varphi; 0, \rho}_{\pi^+p}|T(s)|\underbrace{0, 0; r, \lambda\rangle}_{W^+p}\right)e^{-i\delta_{P_{33}}} \in \mathbb{R} \tag{22}$$

for $r = 0, \pm 1, \lambda = \pm 1/2$, and $M = r - \lambda$. There appear six, in principle, independent amplitudes. The phase of all of them should be $\delta_{P_{33}}$.

Note that $\chi_{r,\lambda}$ in Eq. (22) is given in terms of amplitudes between c.m. states with well-defined 3-momenta and helicities, which could be readily obtained in quantum field theoretical descriptions of the $W^+p \to \pi N$ reaction, such as the HNV model presented in the Introduction. Even for $J = 3/2, I = 3/2$ and only $L = 1$, the HNV model does not fulfill the constraints implicit in Eq. (22).

To improve the HNV model, we (partially) unitarize it in the same fashion as in Refs. [53,54] for pion production induced by real and virtual photons, respectively. We follow the procedure suggested by M. G. Olsson in Ref. [55] and, for every given value of the four-momentum transfer squared q^2, introduce small phases $\Psi_{V,A}(\sqrt{s}, q^2)$, which correct the vector and axial Δ terms in the amplitude.

The matrix element

$$\begin{aligned}&\langle\theta, \varphi; 0, \rho|T(s)|0, 0; r, \lambda\rangle \\ &\quad = \epsilon_{r\mu}T^{\mu}_{\lambda\rho}(\theta, \varphi) \\ &\quad = \epsilon_{r\mu}T^{\mu}_{B\lambda\rho}(\theta, \varphi) + \epsilon_{r\mu}T^{\mu}_{\Delta\lambda\rho}(\theta, \varphi)\end{aligned} \tag{23}$$

can be split into a background (B) and a direct Delta (Δ) contribution. Here, $\epsilon_{r\mu}$ is the polarization vector of the initial W boson. We now follow Ref. [55] and implement Watson's theorem by modifying the above expression to

$$\epsilon_{r\mu}T^{\mu}_{B\lambda\rho}(\theta, \varphi) + e^{i\Psi}\epsilon_{r\mu}T^{\mu}_{\Delta\lambda\rho}(\theta, \varphi) \tag{24}$$

so that

$$\begin{aligned}&\sum_{\rho}(1, 1/2, 3/2|0, -\rho, -\rho) \\ &\quad \times \int d\Omega \mathcal{D}^{(3/2)}_{M-\rho}(\varphi, \theta, -\varphi)(\epsilon_{r\mu}T^{\mu}_{B\lambda\rho}(\theta, \varphi) \\ &\quad + e^{i\Psi}\epsilon_{r\mu}T^{\mu}_{\Delta\lambda\rho}(\theta, \varphi)), \\ &M = r - \lambda\end{aligned} \tag{25}$$

has the right phase, $\delta_{P_{33}}(s)$. As mentioned, the phase Ψ depends on the intermediate Δ^{++} invariant mass $\sqrt{s}$ and q^2. Unfortunately, there is no single phase able to do so for all r, λ values. Next-to–leading contributions in the chiral expansion, which depend explicitly on helicities, would eventually perturbatively restore unitarity at the price of introducing new and uncertain low-energy constants. In addition, the resulting amplitudes would be much more complicated and difficult to handle in Monte Carlo event generators. The practical solution proposed here is to consider two different Olsson phases, Ψ_V and Ψ_A, for the vector and axial parts of the transition amplitude

$$T = T^V - T^A, \tag{26}$$

chosen to unitarize only the dominant vector and axial multipoles. Note that both vector and axial parts of these dominant $W^+p \to p\pi^+$ multipoles are required to fulfill Watson's theorem independently. This is justified because the vector part, which is the only one present in photo- and electropion production amplitudes, should satisfy Watson's theorem independently and therefore have the phase $\delta_{P_{33}}$.

Using invariance under parity, the number of independent amplitudes can be reduced down to three vector and three axial ones (Appendix B) because

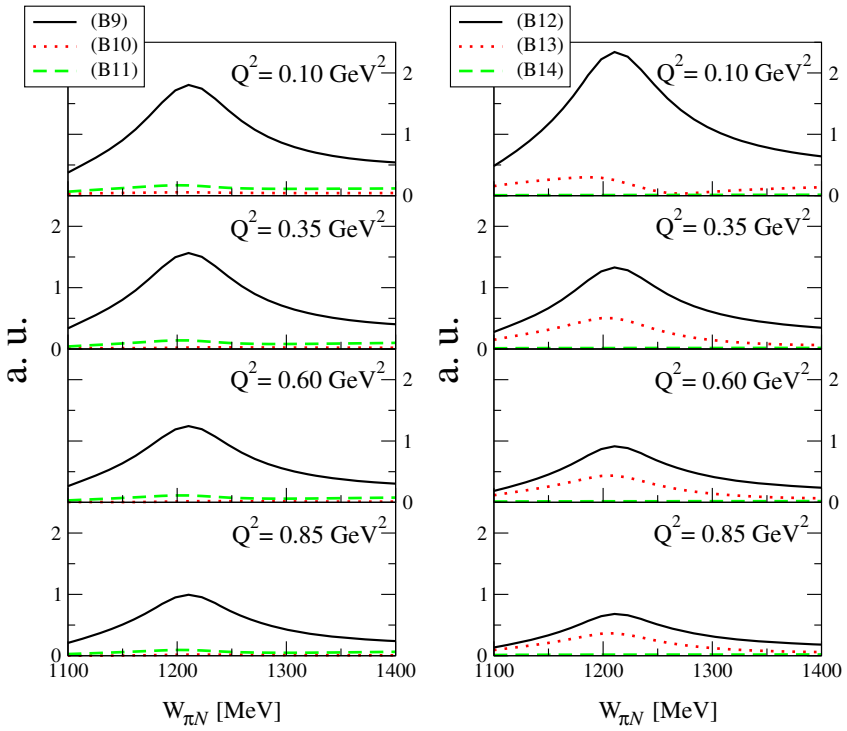

FIG. 1. Modulus of the different vector (left panels) and axial (right panels) multipoles defined in Eqs. (B9)–(B14) of Appendix B. The scale is the same in all panels.

$$\chi_{r,\lambda} = \chi^V_{r,\lambda} - \chi^A_{r,\lambda} = -(\chi^V_{-r,-\lambda} + \chi^A_{-r,-\lambda}). \tag{27}$$

To obtain the vector and axial dominant multipoles, we rewrite the $|3/2, M; L'S'\rangle$ initial WN states in Eq. (B1) in terms of the set of states commonly used in pion electroproduction [56]. Thus, we first couple the WN orbital angular momentum to the W boson spin $(L' \otimes 1)^{\tilde{l}}$ and then the resulting $\tilde{l}$ angular momentum to the nucleon spin to get total angular momentum states with $J = 3/2$. The relation between the new and old states is given in terms of Racah coefficients ($\tilde{W}$),

$$|JM; L'S'\rangle = \sum_{\tilde{l}} \sqrt{(2S'+1)(2\tilde{l}+1)}\, \tilde{W}(1/2, 1, J, L'; S'\tilde{l})|JM; L'\tilde{l}\rangle. \tag{28}$$

The six independent multipoles in this basis are matrix elements of the form

$$\langle L = 1, S = 1/2|T^{V,A}_{J=\frac{3}{2}}(s)|L'\tilde{l}\rangle, \tag{29}$$

with $(L' = 1, \tilde{l} = 1, 2)$ and $(L' = 3, \tilde{l} = 2)$ for the vector part and $(L' = 0, \tilde{l} = 1)$ and $(L' = 2, \tilde{l} = 1, 2)$ for the axial one. The actual relations of these multipoles with the $\chi^{V,A}_{r,\lambda}$ amplitudes can be found in Appendix B [Eqs. (B9)–(B14)].

As discussed above, we impose Watson's theorem only on the dominant vector and axial multipoles given, respectively, by Eqs. (B9) and (B12). These are the magnetic M_{1+} multipole in the vector part [56], $\langle L = 1, S = 1/2|T^V_{J=\frac{3}{2}}(s)|L' = 1\tilde{l} = 1\rangle$, and the WN s-wave $\langle L = 1, S = 1/2|T^A_{J=\frac{3}{2}}(s)|L' = 0\tilde{l} = 1\rangle$ multipole in the axial one. The remaining two matrix elements involve the WN pair in the relative d wave ($L' = 2$). In Fig. 1, we show the modulus of the different vector and axial multipoles defined in Eqs. (B9)–(B14) in Appendix B. The results are very similar after partial unitarization. From Fig. 1, it is apparent that, while the vector multipole of Eq. (B9) remains dominant in the whole q^2 range, the axial multipole of Eq. (B13) becomes comparable to the one of Eq. (B12) as $Q^2 = -q^2$ increases. One might then question the approximation of imposing unitarity for the multipole of Eq. (B12) alone in the axial sector. In this respect, it should be stressed that for larger Q^2 the contributions of both multipoles to the amplitudes become very similar. This is because the terms in which they differ (proportional to $\chi^A_{0,-1/2}$) are suppressed by powers of $1/\sqrt{Q^2}$ from the vector boson polarization for $r = 0$ [Eq. (C5)]. Therefore, once the dominant multipole of Eq. (B12) fulfills Watson's theorem, it is, to a large degree, also fulfilled by the subdominant one of Eq. (B13).

The relative Δ to background phases, $\Psi_V(\sqrt{s}, q^2)$ and $\Psi_A(\sqrt{s}, q^2)$, are fixed by requiring the phase of each of the amplitudes χ^V and χ^A, defined as[7]

[7]Note that the symmetry relations of Eq. (27) guarantee that χ^V (χ^A) depends only on matrix elements of T^V (T^A).

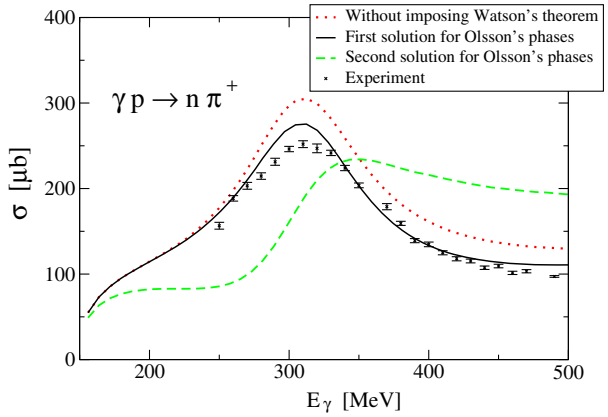

FIG. 2. Results for the $\gamma p \to n\pi^+$ reaction obtained with the vector part of our model. A better description of the experimental data is obtained with the smallest Ψ_V Olsson phase (first solution). Experimental data are taken from Ref. [57].

$$\chi^V = \frac{1}{2}[(\chi_{1,1/2} - \chi_{-1,-1/2}) + \sqrt{3}(\chi_{1,-1/2} - \chi_{-1,1/2})] \quad (30)$$

$$\chi^A = -\frac{1}{\sqrt{6}}[\sqrt{2}(\chi_{0,-1/2} + \chi_{0,1/2}) + \sqrt{3}(\chi_{1,-1/2} + \chi_{-1,1/2}) + (\chi_{1,1/2} + \chi_{-1,-1/2})] \quad (31)$$

to be $\delta_{P_{33}}(s)$. This is to say, we impose

$$\mathrm{Im}[e^{-i\delta_{P_{33}}(s)}\chi^{V,A}] = 0. \quad (32)$$

In each case, there exist two sets of solutions, which correspond to $\chi^{V,A}$ having phases $\delta_{P_{33}}$ and $(\delta_{P_{33}} + \pi)$, respectively (note that the πN phase shift is defined up to a π factor). We take the first set of solutions because it leads to the smallest Ψ_V and Ψ_A Olsson extra phases. The second solution for the vector current is discarded by data on pion photoproduction off nucleons. This is shown in Fig. 2 where we apply the vector part of our model to describe the $\gamma p \to n\pi^+$ reaction. As seen from Fig. 2, a much better agreement with the data is obtained when taking the solution with the smallest Ψ_V Olsson phase. As for Ψ_A, the results shown in Fig. 12 of Appendix B of Ref. [31] favor vector and axial $\Delta(1232)$ contributions having similar phases.

III. RESULTS AND DISCUSSION

We (partially) unitarize the HNV model using Olsson's implementation of Watson's theorem discussed in Sec. II C. For this purpose, we implement the constraints implicit in Eq. (32) using $\chi_{r,\lambda}$ amplitudes calculated by means of Eq. (22). In Appendix C, details on the evaluation of matrix elements $\langle\theta,\varphi;0,\rho|T(s)|0,0;r,\lambda\rangle$, which appears in Eq. (22), within the HNV model are provided. For the P_{33} πN phases, we have used the output of the George Washington University Partial Wave Analysis (SAID) [58] from which we take the WI08 single energy values. In the analysis, we neglect the influence of the small errors (ranging from 0.1% to 0.6%) in the P_{33} phase shifts given in Ref. [58].

A. Fit A

Following Ref. [36], we make a simultaneous fit to both ANL and BNL data samples, taking into account deuterium effects but now imposing the unitarity of the two dominant multipoles $\chi^{V,A}$. This analysis gives (fit A)

$$C_5^A(0) = 1.12 \pm 0.11,$$
$$M_{A\Delta} = (953.7 \pm 62.6)\ \mathrm{MeV}. \quad (33)$$

The new central value of $C_5^A(0)$ agrees within 1σ with the off-diagonal GTR prediction. As in Ref. [36], the ANL [46] flux-averaged $d\sigma/dQ^2$ differential cross section, with a $W_{\pi N} = \sqrt{s} < 1.4$ GeV cut in the final pion-proton invariant mass, and the integrated cross sections for the three lowest neutrino energies (0.65, 0.9, and 1.1 GeV) of the BNL data set [47] have been fitted. A systematic error, due to flux uncertainties (20% for ANL and 10% for BNL data) has been added in quadratures to the statistical one.

In Table I, we compare the results for $C_5^A(0)$ and $M_{A\Delta}$ obtained in this work with those from previous HNV fits

TABLE I. Results from different fits to the ANL and BNL data. All fits include the ANL [46] flux-averaged $d\sigma/dQ^2$ differential cross section, with a $W_{\pi N} = \sqrt{s} < 1.4$ GeV cut, and the integrated cross sections for the three lowest neutrino energies (0.65, 0.9, and 1.1 GeV) of the BNL data set [47]. Fits I*, II*, and IV are taken from Ref. [36]. In all cases, Adler's constraints ($C_3^A = 0$, $C_4^A = -C_5^A/4$) [13,14] are imposed. Deuteron effects [36] are included in fit IV and in those carried out in this work. The nonresonant chiral background contributions are included in all cases, with the exception of fit I*. For $C_5^A(q^2)$, a dipole form, $C_5^A(q^2) = C_5^A(0)/(1 - q^2/M_{A\Delta}^2)^2$, has been used in all fits except in the one carried out in Ref. [31], where an extra factor $1/(1 - q^2/3M_{A\Delta})$ was included [see Eq. (48) of that reference]. Finally, r is the Gaussian correlation coefficient between $C_5^A(0)$ and $M_{A\Delta}$. For reference, the prediction of the GTR is $C_5^A(0) = 1.15 - 1.2$.

	$C_5^A(0)$	$M_{A\Delta}$/GeV	Data	r	χ^2/dof
Ref. [31]	0.867 ± 0.075	0.985 ± 0.082	ANL	−0.85	0.40
Ref. [36]: Fit I* (only Δ pole)	1.08 ± 0.10	0.92 ± 0.06	ANL & BNL	−0.06	0.36
Fit II*	0.95 ± 0.11	0.92 ± 0.08	ANL & BNL	−0.08	0.49
Fit IV (with deuteron effects)	1.00 ± 0.11	0.93 ± 0.07	ANL & BNL	−0.08	0.42
This work (unitarized + deuteron effects) fit A	1.12 ± 0.11	0.954 ± 0.063	ANL & BNL	−0.08	0.46

carried out in Refs. [31,36]. With respect to the fit carried out in Ref. [31], the consideration of BNL data and flux uncertainties in Ref. [36] led to an increased value of $C_5^A(0)$, while strongly reducing the statistical correlations between $C_5^A(0)$ and $M_{A\Delta}$. The inclusion of background terms reduced $C_5^A(0)$, while deuteron effects slightly increased it by about 5%, consistently with the results of Refs. [31] and [24,35]. The implementation of Watson's theorem, for the dominant vector and axial multipoles, in new fit A, further increases the $C_5^A(0)$ value, bringing it into much better agreement with the off-diagonal GTR prediction.

The resulting Olsson phases from fit A are depicted in Fig. 3. In the left panel of Fig. 3, we show the phases Ψ_V, Ψ_A obtained at the Δ peak as a function of Q^2. In the middle and right panels of Fig. 3, we give, for different Q^2 values, the Ψ_V, Ψ_A dependence on the Δ invariant mass $W_{\pi N}$. The vector phase Ψ_V agrees reasonably well with the one determined for electron scattering in Ref. [54].

The results of the (partially) unitarized model derived in this work (fit A) are confronted to the fitted data in Fig. 4. The same good agreement to the data as in Ref. [36], where partial unitarity was not imposed, is now obtained with a higher $C_5^A(0)$ consistent with the GTR. The increase in the $C_5^A(0)$ value with respect to that calculation is compensated by the change in the interference between the dominant Δ term and the background terms once Watson's theorem is imposed on the dominant multipoles.

In Fig. 5, we show the predictions of the partially unitarized (fit A) HNV model for the $\nu_\mu n \to \mu^- p\pi^0$ and $\nu_\mu n \to \mu^- n\pi^+$ channels. They are compared to the ANL and BNL data, assuming that the proton in the deuteron acts as a spectator. The problem with the $\nu_\mu n \to \mu^- n\pi^+$ channel, where data are underestimated in most theoretical models, still persists after partial unitarization. This significant discrepancy deserves additional work, even more so because there exist only two independent amplitudes, and thus the $p\pi^0$ and $p\pi^+$ channels fully determine the $n\pi^+$ amplitude [31]. We would like to point out that the crossed Δ mechanism has a large contribution in the $n\pi^+$ channel. Indeed, besides the Δ propagator, the numerical factors of the (direct and crossed) Δ mechanisms are $(\sqrt{3}\ \&\ 1/\sqrt{3})$, $(2/\sqrt{3}\ \&\ -2/\sqrt{3})$, and $(1/\sqrt{3}\ \&\ \sqrt{3})$ for the $p\pi^+$, $p\pi^0$, and $n\pi^+$ channels, respectively [31]. The spin structure of the Δ propagator used in Ref. [31] suffers from some off-shell ambiguities/inconsistencies, which are clearly enhanced in the evaluation of the crossed term, where the resonance is far

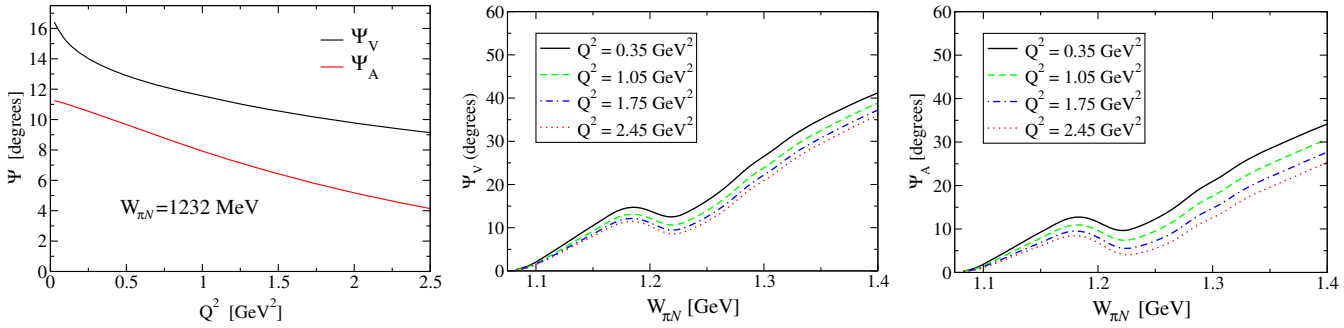

FIG. 3. Olsson phases from fit A. Left panel: Ψ_V and Ψ_A at the Δ peak as a function of $Q^2 = -q^2$. Middle and right panels: Ψ_V and Ψ_A as a function of the Δ invariant mass $W_{\pi N}$ for different Q^2 values, respectively.

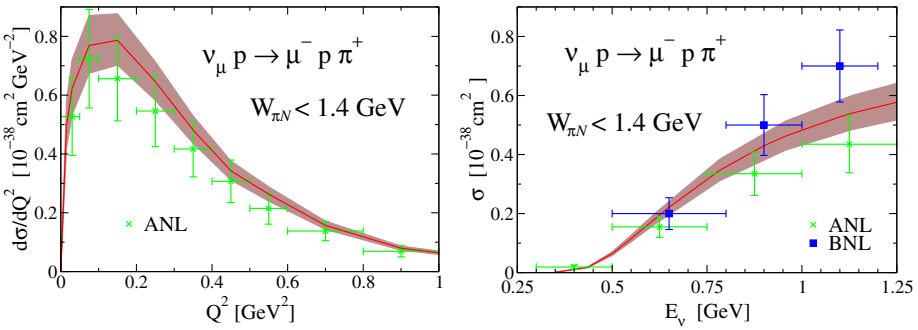

FIG. 4. Results from fit A for the differential $d\sigma/dQ^2$ (left) and total (right) cross section for the $\nu_\mu p \to \mu^- p\pi^+$ reaction compared to the ANL [46] and BNL [47] data. The theoretical bands correspond to the variation of the results when $C_5^A(0)$ changes within the error interval determined from the fit. Experimental data include a systematic error, due to flux uncertainties (20% for ANL and 10% for BNL data), which has been added in quadratures to the statistical ones. Theoretical results and ANL data include a cut in the final pion-proton invariant mass given by $W_{\pi N} < 1.4$ GeV. Deuteron effects have been taken into account assuming that the neutron in the deuteron acts as a spectator (details in Ref. [36]).

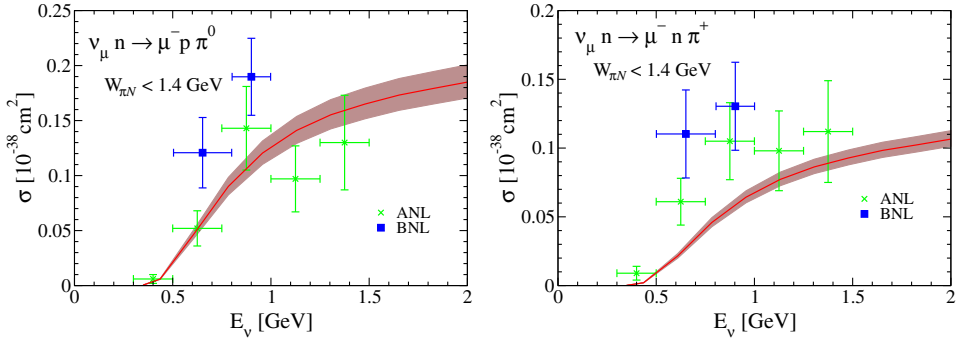

FIG. 5. Results from fit A [Eq. (33)] for the $\nu_\mu n \to \mu^- p\pi^0$ (left panel) and $\nu_\mu n \to \mu^- n\pi^+$ (right panel) total cross sections as compared to ANL [46] and BNL [47] data. Theoretical bands and experimental errors have the same meaning as in Fig. 4. Theoretical results and ANL data include a cut in the final active nucleon-pion invariant mass given by $W_{\pi N} < 1.4$ GeV. Deuteron effects have been taken into account as explained in Ref. [36], assuming that the proton in the deuteron acts as a spectator.

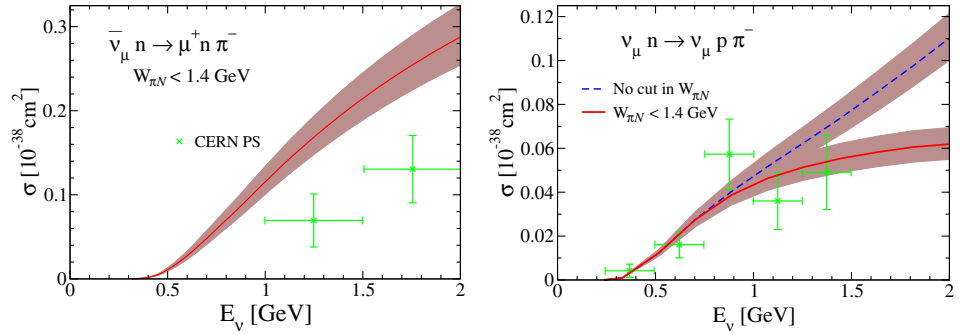

FIG. 6. Results from fit A [Eq. (33)] for the $\bar{\nu}_\mu n \to \mu^+ n\pi^-$ (left panel) and $\nu_\mu n \to \nu_\mu p\pi^-$ (right panel) total cross sections. Data from CERN PS were taken in a freon-propane (CF_3Br—C_3H_8) target [60]. Experimental data for the $\nu_\mu n \to \nu_\mu p\pi^-$ reaction are from Ref. [62]. Since this latter cross section was measured at ANL, we have assumed a 20% systematic error, due to flux uncertainties, that has been added in quadratures to the statistical error. Besides, for the $\nu_\mu n \to \nu_\mu p\pi^-$ case, we have taken into account deuteron effects, as explained in Ref. [36], assuming the proton in the deuteron as a spectator. Theoretical bands have the same meaning as in Fig. 4. Theoretical results, except where indicated, include a cut in the final pion-nucleon invariant mass given by $W_{\pi N} < 1.4$ GeV.

from its mass shell. This might have consequences, which would affect much more the $n\pi^+$ channel than the other two charge configurations. Research along these lines is underway.

Effects of the final state interactions (FSIs) on cross sections for the single pion production off the deuteron should also be considered and might help to explain the puzzling $n\pi^+$ channel. Such effects have been recently examined in the work of Ref. [59]. There, it is found that the orthogonality between the deuteron and final pn scattering wave functions significantly reduces the cross sections. Thus, the ANL and BNL data on the deuterium target might need a more careful analysis with the FSIs taken into account. It is also relevant to incorporate the kinematical cuts implemented in the experiments to properly separate the three reaction channels.

Finally, in Fig. 6, we give the fit A results for the $\bar{\nu}_\mu n \to \mu^+ n\pi^-$ and $\nu_\mu n \to \nu_\mu p\pi^-$ channels. In the first case, we compare with the data from Ref. [60] that were obtained at the CERN proton synchrotron (PS) using a freon-propane (CF_3Br—C_3H_8) target. There is a large discrepancy in this case between the theoretical calculation and the experimental data. As shown in Ref. [61], this can be explained by nuclear medium and pion absorption effects, which were not properly taken into account in the analysis of Ref. [60]. For the second reaction, we find a nice agreement with the experimental data from Ref. [62].

B. Fit B

The ANL and BNL bubble chamber pion production measurements have been recently revisited [63]. Both experiments have been reanalyzed to produce the ratio between the $\sigma(\nu_\mu p \to \mu^- p\pi^+)$ and the charged current quasielastic (CCQE) cross sections measured in deuterium, cancelling in this way the flux uncertainties present in the data. A good agreement between the two experiments for these ratios was found, providing in this way an explanation to the longstanding tension between the two data sets. By multiplying the cross section ratio by the theoretical CCQE cross section on the deuteron,[8] which is well under control, flux normalization independent pion production

[8]They use the prediction from GENIE 2.9 [64].

TABLE II. ANL and BNL integrated cross sections (in units of 10^{-38} cm^2) taken from the reanalysis of Ref. [63] and included in the χ^2 of Eq. (34) (fit B).

E_ν (GeV)	$\sigma\|_{\rm exp}$	$\Delta(\sigma\|_{\rm exp})$	Exp.
0.3	0.0020	0.0020	ANL
0.5	0.070	0.012	ANL
0.7	0.28	0.03	ANL
0.9	0.50	0.06	ANL
0.5	0.056	0.016	BNL
0.7	0.26	0.03	BNL
0.9	0.43	0.04	BNL

cross sections were extracted. We have taken advantage of these developments and performed a new fit considering some of the new data points.

We have minimized

$$\chi^2 = \sum_{i\in \rm ANL} \left(\frac{\beta d\sigma/dQ_i^2|_{\rm exp} - d\sigma/dQ_i^2|_{\rm th}}{\beta \Delta(d\sigma/dQ_i^2|_{\rm exp})} \right)^2 + \sum_{i\in \rm ANL} \left(\frac{\sigma_i|_{\rm exp} - \sigma_i|_{\rm th}}{\Delta(\sigma_i|_{\rm exp})} \right)^2 + \sum_{i\in \rm BNL} \left(\frac{\sigma_i|_{\rm exp} - \sigma_i|_{\rm th}}{\Delta(\sigma_i|_{\rm exp})} \right)^2 . \quad (34)$$

The ANL and BNL integrated cross sections included in the above χ^2, taken from Ref. [63], are collected in Table II. Since no cut in the outgoing pion-nucleon invariant mass was considered in the new analysis of Ref. [63], and in order to avoid heavier resonances from playing a significant role, we have only included data points corresponding to laboratory neutrino energies $E_\nu \leq 1.1$ GeV. To constrain the q^2 dependence, we have also fitted the shape of the original ANL flux-folded $d\sigma/dQ^2$ distribution, not affected by the new analysis of Ref. [63], where a $W_{\pi N} = \sqrt{s} < 1.4$ GeV cut in the final pion-proton invariant mass was implemented. The new best fit parameter β in the first term of Eq. (34) is an arbitrary scale that allows us to consider only the shape of this distribution. In turn, we do not now include any systematic error on the ANL $d\sigma/dQ^2$ differential cross section. As in fit A, we consider deuterium effects and Adler's constraints ($C_3^A = 0$, $C_4^A = -C_5^A/4$) on the axial form factors and for $C_5^A(q^2)$ use the dipole functional form shown in the caption of Table I. Besides, Olsson's approximate implementation of Watson's theorem is also taken into account. The best fit parameters in this case (fit B) are

$$C_5^A(0) = 1.14 \pm 0.07, \qquad M_{A\Delta} = (959.4 \pm 66.9)\ \text{MeV}, \quad (35)$$

with $\beta = 1.19 \pm 0.08$ and $\chi^2/dof = 0.3$. The values for $C_5^A(0)$ and M_A from fit B are very close to the ones obtained in fit A. Without including the Olsson phases, fit B gives a smaller $C_5^A(0) = 1.05 \pm 0.07$ value, in worse agreement with the GTR prediction. This is the same effect seen when comparing fit A with fit IV in Ref. [36]. The value $\beta = 1.19 \pm 0.08$ suggests that ANL results in Ref. [46] could have underestimated the pion production cross sections by some 20% due to neutrino flux uncertainties. A comparison of the theoretical results from fit B and the fitted data is now shown in Fig. 7. Similar results to those from fit A are obtained for the Olsson phases and the cross sections for the other channels.

IV. FINAL REMARKS

Pion production on a deuteron target induced by neutrinos and antineutrinos has been studied using the HNV model [31], which takes into account nonresonant amplitudes, required by chiral symmetry, as well as resonant ones with $\Delta(1232)$ and $N^*(1520)$ intermediate states. Phenomenological form factors allow us to apply the model to finite 4-momentum transfers q^2 probed in neutrino

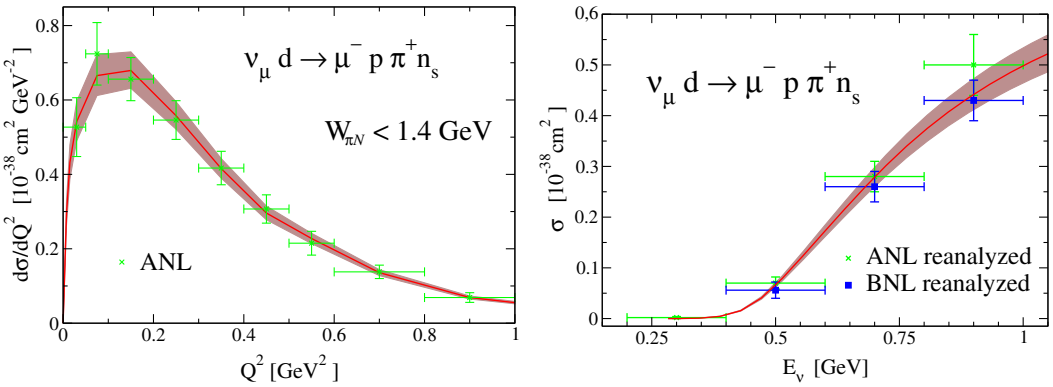

FIG. 7. Results from fit B [Eq. (35)] for the shape of the differential $d\sigma/dQ^2$ (left) and for total cross sections (right) for the $\nu_\mu p \to \mu^- p \pi^+$ reaction compared, respectively, to the ANL [46] data and the ANL and BNL reanalyzed total cross sections of Ref. [63]. Theoretical bands are as in Fig. 4. In the left panel, both experimental data and theoretical results include a cut in the final pion-neutron invariant mass given by $W_{\pi N} < 1.4$ GeV. Besides, theoretical results in the left panel have been divided by $\beta = 1.19$, accounting for flux uncertainties [see Eq. (34)]. Deuteron effects have been taken into account as explained in Ref. [36].

experiments. The model has now been improved by imposing Watson's theorem to the dominant vector and axial multipoles. In this way, unitarity has been partially restored.

With this theoretical tool, we have undertaken a new determination of the leading axial $N\Delta(1232)$ transition form factor from ANL and BNL data. We have fitted not only the original data (fit A) but also those obtained in a recent reanalysis [63] that has removed the tension between the two data sets by considering flux independent ratios (fit B). Both fits A and B show that the partial unitarization increases the value of the leading axial coupling $C_5^A(0)$ with respect to fits where no unitarization was applied. Thanks to the new analysis of Ref. [63], the error in $C_5^A(0)$ has been reduced from 10% (fit A) to 6% (fit B). The agreement with the data is equally satisfactory as in previous fits performed without unitarization, but the new $C_5^A(0)$ values are in better agreement with the prediction from the off-diagonal GTR. One should also mention that the description of pion photoproduction at the $\Delta(1232)$ peak is also improved without refitting the electromagnetic couplings (Fig. 2). It is the new interference pattern between the Δ-pole amplitude and background contributions that compensates for the increase in the $C_5^A(0)$ value. Actually, the results are compatible with the ones obtained in a simpler model where only the dominant Δ mechanism was included and where $C_5^A(0) \approx 1.15$–1.2, as given by the off-diagonal GTR. However, a more complete model containing not only the Δ mechanism but also background terms is definitely more robust. In fact, as shown in Ref. [31], there are parity violating observables that are nonzero only in the presence of background terms.

Full unitarity is also to be preferred. The advantage of the simpler scheme adopted here resides mostly in its simplicity. This would allow for an easier implementation in event generators used in the analysis of neutrino experiments while, at the same time, providing an accurate description of the pion production data for $W_{\pi N} < 1.4$ GeV. The framework is also general enough to correct for deviations from Watson's theorem in more elaborated weak pion production models. The accuracy can be also increased by fixing the phases in other subdominant multipoles.

ACKNOWLEDGMENTS

We thank Callum Wilkinson for making the results of Ref. [63] available to us. This research has been supported by the Spanish Ministerio de Economía y Competitividad (MINECO) and the European fund for regional development (FEDER) under Contracts No. FIS2011-28853-C02-01, No. FIS2011-28853-C02-02, No. FPA2013-47443-C2-2-P, No. FIS2014-51948-C2-1-P, No. FIS2014-51948-C2-2-P, No. FIS2014-57026-REDT, and No. SEV-2014-0398; by Generalitat Valenciana under Contract No. PROMETEOII/2014/0068; and by the European Union HadronPhysics3 project, Grant No. 283286.

APPENDIX A: C.M. TWO-PARTICLE HELICITY STATES

We follow the notation in Ref. [51], up to some trivial factors in the normalization of the states. Particle states are defined by the Poincaré symmetry group Casimir operators. Thus, the states $|m, j, \vec{p}, \lambda\rangle$ are characterized by the mass (m), spin (j), 3-momentum ($\vec{p}$), and helicity[9] (λ) of the particle. They are constructed as

$$|m, j; \vec{p}, \lambda\rangle = R(\varphi, \theta, -\varphi) Z_{|\vec{p}|} |m, j; \vec{0}, \lambda\rangle, \tag{A1}$$

with $Z_{|\vec{p}|}$ being a boost in the positive z direction and $R(\varphi, \theta, -\varphi)$ a rotation that takes that axis into the direction of $\vec{p}$ (θ, φ are the polar and azimuthal angles of $\vec{p}$, $0 \le \theta \le \pi$, $0 \le \varphi < 2\pi$). The state $|\vec{0}, \lambda\rangle$ has $\vec{p} = \vec{0}$ and spin projection along the z axis λ. After the transformations, λ becomes the helicity of the one-particle state. The normalization is such that

$$\langle m, j, \vec{p}, \lambda | m, j, \vec{p}', \lambda' \rangle = (2\pi)^3 2E(\vec{p}) \delta^3(\vec{p} - \vec{p}') \delta_{\lambda\lambda'} \tag{A2}$$

with $E(\vec{p}) = \sqrt{m^2 + \vec{p}^2}$. Helicity c.m. two-particle states are defined as

$$|p, \theta, \varphi; \lambda_1, \lambda_2; \gamma\rangle = |m_1, j_1; \vec{p}, \lambda_1\rangle \otimes \overline{|m_2, j_2; -\vec{p}, \lambda_2\rangle}, \tag{A3}$$

where γ encompasses all other not explicitly identified quantum numbers, and

$$\overline{|m_2, j_2; -\vec{p}, \lambda_2\rangle} = (-1)^{j_2 - \lambda_2} R(\varphi, \theta, -\varphi) R(0, \pi, 0) Z_{|\vec{p}|} |m_2, j_2; \vec{0}, \lambda_2\rangle; \tag{A4}$$

the phase factor $(-1)^{j_2 - \lambda_2}$ is introduced so that as $\vec{p} \to 0$

$$\overline{|m_2, j_2; \vec{p} = \vec{0}, \lambda_2\rangle} = |m_2, j_2; \vec{p} = \vec{0}, -\lambda_2\rangle. \tag{A5}$$

Defining the two-particle state in this way guarantees good transformation properties under rotations

$$|p, \theta, \varphi; \lambda_1, \lambda_2; \gamma\rangle = R(\varphi, \theta, -\varphi) |p, 0, 0; \lambda_1, \lambda_2; \gamma\rangle. \tag{A6}$$

It is convenient to decompose

$$|p, \theta, \varphi; \lambda_1, \lambda_2; \gamma\rangle = 2\pi \sqrt{\frac{4\sqrt{s}}{|\vec{p}|}} |P\rangle |\theta, \varphi; \lambda_1, \lambda_2; \gamma\rangle, \tag{A7}$$

[9]Spin component along the direction of motion.

with P the total four-momentum and $P^2 = s$. The normalizations are[10]

$$\langle P'|P\rangle = (2\pi)^4\delta^4(P-P'),$$
$$\langle\theta',\varphi';\lambda_1',\lambda_2';\gamma'|\theta,\varphi;\lambda_1,\lambda_2;\gamma\rangle = \delta(\Omega-\Omega')\delta_{\lambda_1\lambda_1'}\delta_{\lambda_2\lambda_2'}\delta_{\gamma\gamma'}. \tag{A8}$$

The decomposition in Eq. (A7) attends to the fact the 4-momentum is a conserved quantity and thus

$$\langle F|S|I\rangle = (2\pi)^4\delta^4(P_F-P_I)\langle\alpha_F|S_P|\alpha_I\rangle \tag{A9}$$

and any state of the Hilbert space, containing any number of particles, can be written as a superposition of vectors of the form $|P\rangle|\alpha\rangle$. The set of vectors $|\alpha\rangle$ spans the so-called little Hilbert space [51]. It follows that the scattering operator S may be written as the direct product

$$S = \mathbb{1}\otimes S_P \tag{A10}$$

such that

$$\langle F|S|I\rangle = \langle P_F|\mathbb{1}|P_I\rangle\langle\alpha_F|S_P|\alpha_I\rangle. \tag{A11}$$

Just as in the case of the S operator, T may also be written as a direct product,

$$T = \mathbb{1}\otimes T_P, \qquad S_P = \mathbb{1} - iT_P. \tag{A12}$$

This is the form in which the T matrix is generally used. In fact, we refer to T_P as the T operator and $T_{FI}(s) = \langle\alpha_F|T_P|\alpha_I\rangle$ as the T matrix element.

The c.m. states can be written in terms of states with well-defined total angular momentum,

$$|p,J,M;\lambda_1,\lambda_2;\gamma\rangle = 2\pi\sqrt{\frac{4\sqrt{s}}{|\vec{p}|}}|P\rangle|J,M;\lambda_1,\lambda_2;\gamma\rangle, \tag{A13}$$

with

$$\langle J',M';\lambda_1',\lambda_2';\gamma'|J,M;\lambda_1,\lambda_2;\gamma\rangle = \delta_{JJ'}\delta_{MM'}\delta_{\lambda_1\lambda_1'}\delta_{\lambda_2\lambda_2'}\delta_{\gamma\gamma'}. \tag{A14}$$

Starting from the case $\theta = 0$, $\varphi = 0$,

$$|0,0;\lambda_1,\lambda_2;\gamma\rangle = \sum_J C_J|J,J_z=\lambda;\lambda_1,\lambda_2;\gamma\rangle, \tag{A15}$$

with $\lambda = \lambda_1 - \lambda_2$, one arrives at

$$|\theta,\varphi;\lambda_1,\lambda_2;\gamma\rangle = \sum_{J,M} C_J\mathcal{D}^{(J)}_{M\lambda}(\varphi,\theta,-\varphi)|J,M;\lambda_1,\lambda_2;\gamma\rangle, \qquad \lambda = \lambda_1-\lambda_2, \tag{A16}$$

where $\mathcal{D}^{(J)}_{MM'}(\alpha,\beta,\gamma)$ is the matrix representation of a rotation operator $R(\alpha,\beta,\gamma)$ in an irreducible representation space,

$$\mathcal{D}^{(J)}_{M'M}(\alpha,\beta,\gamma) = e^{-i\alpha M'}d^J_{M'M}(\beta)e^{-i\gamma M},$$
$$d^J_{M'M}(\beta) = \langle JM'|e^{-i\beta J_y}|JM\rangle. \tag{A17}$$

From the above equation and using that

$$\int d\Omega\mathcal{D}^{(J)*}_{M\lambda}(\varphi,\theta,-\varphi)\mathcal{D}^{(J')}_{M'\lambda}(\varphi,\theta,-\varphi) = \frac{4\pi}{2J+1}\delta_{JJ'}\delta_{MM'}, \tag{A18}$$

it follows that

$$\begin{aligned}|J,M;\lambda_1,\lambda_2;\gamma\rangle &= \frac{2J+1}{4\pi C_J}\int d\Omega\mathcal{D}^{(J)*}_{M\lambda}(\varphi,\theta,-\varphi)|\theta,\varphi;\lambda_1,\lambda_2;\gamma\rangle\\ &= \sqrt{\frac{2J+1}{4\pi}}\int d\Omega\mathcal{D}^{(J)*}_{M\lambda}(\varphi,\theta,-\varphi)|\theta,\varphi;\lambda_1,\lambda_2;\gamma\rangle, \qquad \lambda=\lambda_1-\lambda_2,\end{aligned} \tag{A19}$$

where we have made use of the normalization conditions to determine $|C_J|^2 = \frac{2J+1}{4\pi}$ and have taken the coefficients C_J to be real. States with well-defined orbital angular momentum L and spin S can be introduced as

$$|J,M;\lambda_1,\lambda_2;\gamma\rangle = \sum_{L,S}\sqrt{\frac{2L+1}{2J+1}}(L,S,J|0,\lambda,\lambda)(j_1,j_2,S|\lambda_1,-\lambda_2,\lambda)|J,M;L,S;\gamma\rangle,$$
$$|J,M;L,S;\gamma\rangle = \sum_{\lambda_1,\lambda_2}\sqrt{\frac{2L+1}{2J+1}}(L,S,J|0,\lambda,\lambda)(j_1,j_2,S|\lambda_1,-\lambda_2,\lambda)|J,M;\lambda_1,\lambda_2;\gamma\rangle, \tag{A20}$$

where $(j_1,j_2,j|m_1,m_2,M)$ are the Clebsch-Gordan coefficients and $\lambda = \lambda_1 - \lambda_2$ as usual.

[10]Note that $E_1E_2\delta^3(\vec{p}_1-\vec{p}_2)\delta^3(\vec{p}_1'-\vec{p}_2') = \sqrt{s}\delta^4(P-P')\delta^2(\Omega-\Omega')/|\vec{p}|$, with $\vec{p} = (\vec{p}_1-\vec{p}_2)/2$.

APPENDIX B: PROPERTIES OF THE $\chi_{r,\lambda}$ AMPLITUDES DEFINED IN EQ. (21)

The $\chi_{r,\lambda}$ amplitudes in Eq. (21) can be rewritten in terms of states $|J,M;L,S\rangle$ with well-defined total orbital (L) and spin (S) angular momenta as

$$\begin{aligned}\chi_{r,\lambda} &= \sqrt{\frac{3}{8}}\sum_{\rho}(1,1/2,3/2|0,-\rho,-\rho)\langle 3/2,M;0,\rho|T(s)|3/2,M;r,\lambda\rangle \\ &= \frac{1}{\sqrt{2}}\langle 3/2,M;L=1,S=1/2|T(s)|3/2,M;r,\lambda\rangle \\ &= \sum_{L',S'}\sqrt{\frac{2L'+1}{8}}(1,1/2,S'|r,-\lambda,M)(L',S',3/2|0,M,M)\langle L=1,S=1/2|T_{J=\frac{3}{2}}(s)|L'S'\rangle,\end{aligned} \tag{B1}$$

with $M=r-\lambda$. Note that the matrix element of the T-scattering operator does not depend on M, since it is invariant under rotations. Now, the amplitude has a vector and an axial part,

$$T = T^V - T^A, \tag{B2}$$

and under a parity transformation, we have

$$\mathcal{P}T\mathcal{P}^\dagger = T^V + T^A \tag{B3}$$

$$\mathcal{P}|J,M;LS\rangle = \eta_1\eta_2(-1)^L|J,M;L,S\rangle, \tag{B4}$$

where $\eta_{1,2}$ are the intrinsic parities of the particles (1 for nucleons and -1 for π and W). We thus find that only odd (even) L' waves contribute to the vector (axial) part of the $\chi_{r,\lambda}$,

$$\chi_{r,\lambda} = \chi^V_{r,\lambda} - \chi^A_{r,\lambda} \tag{B5}$$

$$\chi^V_{r,\lambda} = \sum_{S'=1/2,3/2}\sum_{L'=1,3}\sqrt{\frac{2L'+1}{8}}(1,1/2,S'|r,-\lambda,M)(L',S',3/2|0,M,M)\langle L=1,S=1/2|T^V_{J=\frac{3}{2}}(s)|L'S'\rangle \tag{B6}$$

$$\chi^A_{r,\lambda} = \sum_{S'=1/2,3/2}\sum_{L'=0,2}\sqrt{\frac{2L'+1}{8}}(1,1/2,S'|r,-\lambda,M)(L',S',3/2|0,M,M)\langle L=1,S=1/2|T^A_{J=\frac{3}{2}}(s)|L'S'\rangle. \tag{B7}$$

Now, taking into account

$$(1,1/2,S'|r,-\lambda,M)(L',S',3/2|0,M,M) = (-1)^{L'}(1,1/2,S'|-r,\lambda,-M)(L',S',3/2|0,-M,-M), \tag{B8}$$

we trivially find Eq. (27).

On the other hand, using the basis introduced in Eq. (28), we obtain the following relations[11]:

$$-\frac{1}{2}\langle L=1,S=1/2|T^V_{J=3/2}|L'=1,\tilde{l}=1\rangle = \frac{1}{2}(\chi^V_{1,1/2}+\sqrt{3}\chi^V_{1,-1/2}), \qquad [M_{1+}] \tag{B9}$$

$$-\frac{1}{2}\langle L=1,S=1/2|T^V_{J=3/2}|L'=1,\tilde{l}=2\rangle = \frac{1}{\sqrt{20}}(2\sqrt{2}\chi^V_{0,-1/2}+\sqrt{3}\chi^V_{1,-1/2}-3\chi^V_{1,1/2}), \qquad [E_{1+}/L_{1+}] \tag{B10}$$

$$-\frac{1}{2}\langle L=1,S=1/2|T^V_{J=3/2}|L'=3,\tilde{l}=2\rangle = \frac{1}{\sqrt{10}}(-\sqrt{6}\chi^V_{0,-1/2}+\chi^V_{1,-1/2}-\sqrt{3}\chi^V_{1,1/2}), \qquad [E_{1+}/L_{1+}] \tag{B11}$$

[11]For matrix elements of the vector current, the involved multipoles in the notation of Ref. [56] are shown in square brackets.

$$-\frac{1}{2}\langle L=1,S=1/2|T^A_{J=3/2}|L'=0,\tilde{l}=1\rangle = -\frac{1}{\sqrt{6}}(\sqrt{2}\chi^A_{0,-1/2}+\sqrt{3}\chi^A_{1,-1/2}+\chi^A_{1,1/2}) \quad \text{(B12)}$$

$$-\frac{1}{2}\langle L=1,S=1/2|T^A_{J=3/2}|L'=2,\tilde{l}=1\rangle = -\frac{1}{\sqrt{12}}(-2\sqrt{2}\chi^A_{0,-1/2}+\sqrt{3}\chi^A_{1,-1/2}+\chi^A_{1,1/2}) \quad \text{(B13)}$$

$$-\frac{1}{2}\langle L=1,S=1/2|T^A_{J=3/2}|L'=2,\tilde{l}=2\rangle = -\frac{1}{2}(\chi^A_{1,-1/2}-\sqrt{3}\chi^A_{1,1/2}). \quad \text{(B14)}$$

APPENDIX C: COMPUTATION OF THE $\chi_{r,\lambda}(s)$ AMPLITUDES WITHIN THE HNV MODEL

Equation (22) allows us to compute $\chi_{r,\lambda}(s)$ in terms of the matrix elements $\underbrace{\langle\theta,\varphi;0,\rho|}_{\pi^+p}T(s)\underbrace{|0,0;r,\lambda\rangle}_{W^+p}$, which involve the helicity c.m. two-particle states introduced in Eq. (A3). We have always labeled the proton as the second particle. This is to say that the "bar" $\overline{|j;-\vec{p},\lambda\rangle}$ states correspond to the protons. One can prove that

$$\overline{|j;-\vec{p},\lambda\rangle} = (-1)^{j-\lambda}(-1)^{2j}e^{-2i\lambda\varphi}|j;-\vec{p},\lambda\rangle \quad \text{(C1)}$$

with

$$|j;-\vec{p},\lambda\rangle = R(\varphi+\pi,\pi-\theta,-\varphi-\pi)Z_{|\vec{p}|}|j;\vec{0},\lambda\rangle, \quad \text{(C2)}$$

where θ and φ are the polar and azimuthal angles of $\vec{p}$. The latter states, $|j;-\vec{p},\lambda\rangle$ for the case of a nucleon $j=1/2$, can be easily obtained using the Dirac space representations of the boost and the rotation that appears in Eq. (C2). Finally, and using Eq. (C1), we find that the spinors corresponding to the bar states are

$$\overline{|-\vec{p},\lambda=1/2\rangle} \equiv \sqrt{E+M_N}\begin{pmatrix} -\sin\frac{\theta}{2}e^{-i\varphi} \\ \cos\frac{\theta}{2} \\ -\frac{|\vec{p}|}{E+M_N}\sin\frac{\theta}{2}e^{-i\varphi} \\ \frac{|\vec{p}|}{E+M_N}\cos\frac{\theta}{2}\end{pmatrix} \quad \text{(C3)}$$

$$\overline{|-\vec{p},\lambda=-1/2\rangle} \equiv \sqrt{E+M_N}\begin{pmatrix} \cos\frac{\theta}{2} \\ \sin\frac{\theta}{2}e^{i\varphi} \\ -\frac{|\vec{p}|}{E+M_N}\cos\frac{\theta}{2} \\ -\frac{|\vec{p}|}{E+M_N}\sin\frac{\theta}{2}e^{i\varphi}\end{pmatrix}, \quad \text{(C4)}$$

with M_N the nucleon mass and $E=\sqrt{M_N^2+\vec{p}^2}$. On the other hand, the virtual gauge boson helicity states, when the W 3- momentum is in the positive z direction, read

$$\epsilon^\mu(|\vec{p}|,r=0) = \left(|\vec{p}|/\sqrt{Q^2},0,0,\sqrt{\vec{p}^2-Q^2}/\sqrt{Q^2}\right) \quad \text{(C5)}$$

$$\epsilon^\mu(|\vec{p}|,r=\pm1) = \frac{\mp1}{\sqrt{2}}(0,1,\pm i,0), \quad \text{(C6)}$$

with $-Q^2$, the virtual mass of the gauge boson, i.e., its 4-momentum squared. We only consider the three polarizations that are orthogonal to the W 4-momentum since our analysis in Secs. II B and II C implicitly assumes a positive invariant mass squared for the W boson. The results are then analytically continued to negative invariant masses squared.

With all of these ingredients, within the HNV model, we deduce that, up to an overall real normalization constant that does not affect its phase,

$$\langle\theta,\varphi;0,\rho|T(s)|0,0;r,\lambda\rangle \sim -i[j_\mu(\rho,\lambda)\epsilon^\mu(|\vec{p}|,r)], \quad \text{(C7)}$$

where the $p\pi^+$ current j^μ is taken from Eq. (51) of Ref. [31] and Eq. (A6) of Ref. [9], replacing the proton spinors $u(\vec{p})$ by the bar states of Eqs. (C3) and (C4) corresponding[12] to the helicities ρ and λ. The current of Eq. (A6) of Ref. [9] accounts for the crossed $N(1520)$ pole mechanism, which gives a quite small contribution for the πN invariant masses studied in this work. Note that the direct $N^*(1520)$ excitation mechanism also considered in Ref. [9] does not contribute to the isospin $3/2$ channel.

Note that in the definition of the current j^μ in Refs. [9,31], the factor i from the weak vertex is not included. Actually the gauge coupling is not included either. According to our normalizations, one has $-iT_{\rm aux}=i\mathcal{L}\propto ij^\mu\epsilon_\mu$, and thus, up to real constants, $T_{\rm aux}$ is given by $-j\cdot\epsilon$. The extra i ($iT_{\rm aux}=T$) in Eq. (C7) is included to ensure that Eq. (14) that leads to Eqs. (13) and (15) is satisfied. This is needed because in our conventions the pion and the W gauge boson intrinsic time reversal phases are different (-1 and 1, respectively). To keep Eq. (14) correct, one should add a phase i to the πN state, which compensates the pion odd intrinsic time reversal[13] thanks to the antiunitary character of the time-reversal operator in Eq. (14).

In addition and to implement Watson's theorem, within the approximate Olsson scheme discussed in Sec. II C, the vector and axial direct Δ contributions should be multiplied by the Olsson phases, Ψ_V and Ψ_A.

[12]Obviously, the $\bar{u}$ spinor that appears in Eq. (51) of Ref. [31] should be evaluated using Eqs. (C3) and (C4), taking Hermitian conjugation (†) and multiplying by the γ^0 Dirac matrix.

[13]This is easy to see, for instance, by looking at the πNN Lagrangian in Eq. (26) of Ref. [31] and considering the transformation under time reversal of the nucleon axial current and the derivative operator.

APPENDIX D: PARAMETRIZATIONS OF THE Ψ_V AND Ψ_A OLSSON PHASES

In the following, we give parametrizations for the Ψ_V and Ψ_A Olsson phases, as a function of $w = W_{\pi N} - 1.0779$ GeV and $Q^2 = -q^2$, valid in the intervals $W_{\pi N} \in [1.1, 1.4]$ GeV, $Q^2 \in [0, 2.5]$ GeV^2:

(1) Fit A:

$$\Psi_V = 5w\left(8.3787 + \frac{2.7315 - 25.5185w}{0.05308416 + (0.62862 - 5w)^2} + 301.925w - 985.80w^2 + 862.025w^3\right) \times ((1. + 0.14163Q^2)^{-2} + (0.066192 + w(-0.34057 + 1.631475w))Q^2), \tag{D1}$$

$$\Psi_A = 5w\left(5.2514 + \frac{2.9102 - 26.5085w}{0.0531901969 + (0.63033 - 5w)^2} + 266.565w - 814.575w^2 + 624.05w^3\right) \times ((1. + 0.088539Q^2)^{-2} + (0.026654 + w(-1.17305 + 3.66475w))Q^2). \tag{D2}$$

(2) Fit B:

$$\Psi_A = 5w\left(4.9703 + \frac{2.929 - 26.6295w}{0.0531256401 + (0.63051 - 5w)^2} + 264.27w - 798.525w^2 + 598.85w^3\right) \times ((1. + 0.10152Q^2)^{-2} + (0.041484 + w(-1.20715 + 3.7545w))Q^2), \tag{D3}$$

while Ψ_V is the same as for fit A.

[1] J. G. Morfin, J. Nieves, and J. T. Sobczyk, Adv. High Energy Phys. **2012**, 1 (2012).
[2] J. Formaggio and G. Zeller, Rev. Mod. Phys. **84**, 1307 (2012).
[3] L. Alvarez-Ruso, Y. Hayato, and J. Nieves, New J. Phys. **16**, 075015 (2014).
[4] A. A. Aguilar-Arevalo *et al.* (MiniBooNE Collaboration), Phys. Rev. D **81**, 013005 (2010).
[5] A. Aguilar-Arevalo *et al.* (MiniBooNE Collaboration), Phys. Rev. D **83**, 052009 (2011).
[6] A. Aguilar-Arevalo *et al.* (MiniBooNE Collaboration), Phys. Rev. D **83**, 052007 (2011).
[7] T. Le *et al.* (for the MINERvA Collaboration), Phys. Lett. B **749**, 130 (2015).
[8] O. Lalakulich and U. Mosel, Phys. Rev. C **87**, 014602 (2013).
[9] E. Hernández, J. Nieves, and M. J. V. Vacas, Phys. Rev. D **87**, 113009 (2013).
[10] J. Y. Yu, E. A. Paschos, and I. Schienbein, Phys. Rev. D **91**, 054038 (2015).
[11] J. T. Sobczyk and J. Zmuda, Phys. Rev. C **91**, 045501 (2015).
[12] U. Mosel, Phys. Rev. C **91**, 065501 (2015).
[13] S. L. Adler, Ann. Phys. (N.Y.) **50**, 189 (1968).
[14] J. Bijtebier, Nucl. Phys. **B21**, 158 (1970).
[15] P. A. Zucker, Phys. Rev. D **4**, 3350 (1971).
[16] C. Llewellyn Smith, Phys. Rep. **3**, 261 (1972).
[17] P. A. Schreiner and F. Von Hippel, Nucl. Phys. **B58**, 333 (1973).
[18] T. Alevizos, A. Celikel, and N. Dombey, J. Phys. G **3**, 1179 (1977).
[19] G. L. Fogli and G. Nardulli, Nucl. Phys. **B160**, 116 (1979).
[20] G. L. Fogli and G. Nardulli, Nucl. Phys. **B165**, 162 (1980).
[21] D. Rein and L. M. Sehgal, Ann. Phys. (N.Y.) **133**, 79 (1981).
[22] T. R. Hemmert, B. R. Holstein, and N. C. Mukhopadhyay, Phys. Rev. D **51**, 158 (1995).
[23] L. Alvarez-Ruso, S. Singh, and M. V. Vacas, Phys. Rev. C **57**, 2693 (1998).
[24] L. Alvarez-Ruso, S. Singh, and M. V. Vacas, Phys. Rev. C **59**, 3386 (1999).
[25] M. D. Slaughter, Nucl. Phys. **A703**, 295 (2002).
[26] B. Golli, S. Sirca, L. Amoreira, and M. Fiolhais, Phys. Lett. B **553**, 51 (2003).
[27] T. Sato, D. Uno, and T. Lee, Phys. Rev. C **67**, 065201 (2003).
[28] E. A. Paschos, J.-Y. Yu, and M. Sakuda, Phys. Rev. D **69**, 014013 (2004).
[29] O. Lalakulich and E. A. Paschos, Phys. Rev. D **71**, 074003 (2005).
[30] O. Lalakulich, E. A. Paschos, and G. Piranishvili, Phys. Rev. D **74**, 014009 (2006).
[31] E. Hernandez, J. Nieves, and M. Valverde, Phys. Rev. D **76**, 033005 (2007).
[32] K. M. Graczyk and J. T. Sobczyk, Phys. Rev. D **77**, 053001 (2008).
[33] T. Leitner, O. Buss, L. Alvarez-Ruso, and U. Mosel, Phys. Rev. C **79**, 034601 (2009).
[34] C. Barbero, G. L. Castro, and A. Mariano, Phys. Lett. B **664**, 70 (2008).

[35] K. Graczyk, D. Kielczewska, P. Przewlocki, and J. Sobczyk, Phys. Rev. D **80**, 093001 (2009).
[36] E. Hernandez, J. Nieves, M. Valverde, and M. V. Vacas, Phys. Rev. D **81**, 085046 (2010).
[37] O. Lalakulich, T. Leitner, O. Buss, and U. Mosel, Phys. Rev. D **82**, 093001 (2010).
[38] B. D. Serot and X. Zhang, Phys. Rev. C **86**, 015501 (2012).
[39] C. Barbero, G. L. Castro, and A. Mariano, Phys. Lett. B **728**, 282 (2014).
[40] J. Zmuda and K. Graczyk, AIP Conf. Proc. **1680**, 020013 (2015).
[41] S. Nakamura, H. Kamano, and T. Sato, Phys. Rev. D **92**, 074024 (2015).
[42] M. R. Alam, M. S. Athar, S. Chauhan, and S. K. Singh, arXiv:1509.08622.
[43] R. Feynman, M. Kislinger, and F. Ravndal, Phys. Rev. D **3**, 2706 (1971).
[44] J. Liu, N. C. Mukhopadhyay, and L.-s. Zhang, Phys. Rev. C **52**, 1630 (1995).
[45] D. Barquilla-Cano, A. J. Buchmann, and E. Hernandez, Phys. Rev. C **75**, 065203 (2007); **77**, 019903(E) (2008).
[46] G. Radecky *et al.*, Phys. Rev. D **25**, 1161 (1982).
[47] T. Kitagaki *et al.*, Phys. Rev. D **34**, 2554 (1986).
[48] K. M. Graczyk, J. Zmuda, and J. T. Sobczyk, Phys. Rev. D **90**, 093001 (2014).
[49] K. M. Watson, Phys. Rev. **88**, 1163 (1952).
[50] H. Kamano, S. Nakamura, T.-S. Lee, and T. Sato, Phys. Rev. D **86**, 097503 (2012).
[51] A. Martin and T. Spearman, *Elementary Particle Theory* (North-Holland, Amsterdam, 1970).
[52] W. Gibson and B. Pollard, *Symmetry Principles Particle Physics*, Cambridge Monographs on Physics (Cambridge University Press, Cambridge, England, 1980).
[53] R. Carrasco and E. Oset, Nucl. Phys. **A536**, 445 (1992).
[54] A. Gil, J. Nieves, and E. Oset, Nucl. Phys. **A627**, 543 (1997).
[55] M. Olsson, Nucl. Phys. **B78**, 55 (1974).
[56] D. Drechsel and L. Tiator, J. Phys. G **18**, 449 (1992).
[57] T. Fujii, T. Kondo, F. Takasaki, S. Yamada, S. Homma, K. Huke, S. Kato, H. Okuno, I. Endo, and H. Fujii, Nucl. Phys. **B120**, 395 (1977).
[58] SAID, http://gwdac.phys.gwu.edu/analysis/pin_analysis.html.
[59] J.-J. Wu, T. Sato, and T. S. H. Lee, Phys. Rev. C **91**, 035203 (2015).
[60] T. Bolognese, J. Engel, J. Guyonnet, and J. Riester, Phys. Lett. B **81**, 393 (1979).
[61] M. S. Athar, S. Ahmad, and S. Singh, Phys. Rev. D **75**, 093003 (2007).
[62] M. Derrick *et al.*, Phys. Lett. B **92**, 363 (1980).
[63] C. Wilkinson, P. Rodrigues, S. Cartwright, L. Thompson, and K. McFarland, Phys. Rev. D **90**, 112017 (2014).
[64] C. Andreopoulos *et al.*, Nucl. Instrum. Methods Phys. Res., Sect. A **614**, 87 (2010).